Journal of Quantitative Spectroscopy & Radiative Transfer 222–223 (2019) 115–121

Contents lists available at ScienceDirect

Journal of Quantitative Spectroscopy & Radiative Transfer

journal homepage: www.elsevier.com/locate/jqsrt

Near-field radiative heat transfer enhancement using natural hyperbolic material

Hakan Salihoglu, Xianfan Xu*

School of Mechanical Engineering and Birck Nanotechnology Center, Purdue University, West Lafayette, IN 47907, USA

ARTICLE INFO

Article history:
Received 12 July 2018
Revised 10 September 2018
Accepted 14 October 2018
Available online 16 October 2018

Keywords:
Near-field radiative transfer
Hyperbolic modes
Surface phonon polaritons

ABSTRACT

Hyperbolic materials have been newly discovered that can enhance near-field radiative transfer. Multilayer and three-dimensional hyperbolic materials require challenging fabrication techniques. From a practical point of view, natural hyperbolic materials serve better in applications requiring near-field radiative transfer enhancement. In this study, we investigate enhancement of near-field radiative transfer using natural hyperbolic material – calcite, and compare with that from (also natural) polar dielectric materials, SiC, where phonon polaritons are responsible for enhanced near-field heat transfer. Spectral analyses of enhanced near-field radiative transfer from hyperbolic modes in hyperbolic materials and surface phonon polaritons in polar dielectric materials are carried out and compared, which determine the origin and amount of near-field radiative transfer enhancement in these materials.

1. Introduction

For over a century, it was established that thermal radiation is governed by the Stephan Boltzmann's law and not exceeding the blackbody radiation limit. However, when two bodies are brought to a distance less than the characteristic radiation wavelength determined by the Wien's displacement law, it has been predicted theoretically [1–4] and proven experimentally [5–15] that near-field radiation is much enhanced, and surpasses blackbody radiation. Hence, near-field radiation has become an exciting exploratory area for heat transfer enhancement. Exploiting the near-field radiation behavior, various applications have been proposed such as negative luminescent [16], thermoradiative energy conversion [17,18], radiative cooling [19], thermal spectroscopy [20–22], thermophotovoltaic [23], thermal refrigeration [24], thermal rectifier [25–28], thermotronics [29] and boolean operation [30]. However, convenient implementation methods are also needed.

One of the most recent materials studied for near-field heat transfer enhancement is hyperbolic material [31–36], where the governing mechanism enabling near-field enhancement is the hyperbolic modes. Hyperbolic materials are so named because of their topology of isofrequency surface [37], and wavevector range supported inside the hyperbolic materials extends to infinity within hyperbolic bands, hence called high-κ modes. Due to variations in intramolecular or intermolecular bond strengths, the dielectric response of hyperbolic materials is relatively independent with respect to principal axes, and electromagnetic radiation propagating through hyperbolic material is subjected to negative and positive dielectric responses simultaneously. The Reststrahlen dispersion relation in one of the principal components of permittivity tensor modifies the isofrequency surface, producing a hyperboloid that supports high-κ modes inside the material within certain frequency bands (Reststrahlen bands). These modes are the main source of near-field enhancement at the interfaces between the hyperbolic material/vacuum/hyperbolic material. Hyperbolic materials were first constructed using hybrid layered structures [38–40] or 3D structures [41,42]. However, natural hyperbolic materials also exist including hBN, calcite, and Bi_2Se_3 [43]. Compared to the fabrication challenges of layered and 3D hybrid material structures, natural hyperbolic materials are easier to implement for applications. Field confinement enables the use of natural hyperbolic materials in sub-diffraction imaging and super-resolution focusing [44]. For radiative heat transfer, hBN [45] and calcite are promising due to their low losses ($\varepsilon'' \sim 0.1$) and thus suitable for long-distance transport of radiative heat flux [32] within certain frequency bands that support the hyperbolic modes.

Another class of (natural) material that has been investigated extensively for near-field radiative transfer is polar dielectric materials, where the governing mechanism is the coupling of surface phonon polaritons (SPhP) excited by photons [46–53]. Being a surface phenomenon, these polaritons propagate along interface. In contrast to hyperbolic materials with directional dependency, these polar materials are usually isotropic. Along the polar dielectric surface, surface waves originate from negative dielectric permittivity in the Reststrahlen band where $\varepsilon \leq 0$, but fades away in the

* Corresponding author.
E-mail address: xxu@ecn.purdue.edu (X. Xu).

https://doi.org/10.1016/j.jqsrt.2018.10.022
0022-4073/

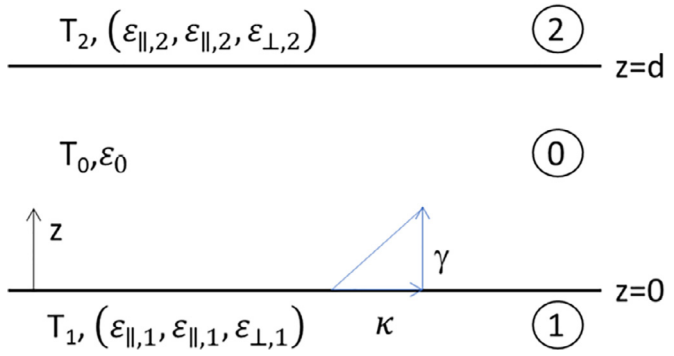

Fig. 1. Schematic of semi-infinite plates separated by vacuum. Here, for uniaxial material, optical axis is along z-axis. Medium 0 is vacuum ($\varepsilon_0 = 1$).

direction perpendicular to the interface, and hence needs to be coupled to another nearby surface for heat extraction [6]. SPhP resonance also leads to quasi-monochromatic thermal emission by means of structured surfaces [54]. Furthermore, studies showed that grating structures on the interface with spatial coherence enable directional thermal radiation [46]. Due to SPhP and low losses compared to metals, polar dielectrics are also preferred in building hybrid hyperbolic materials [37].

This study is devoted to examining contributions to near-field radiative heat transfer by the hyperbolic modes in natural hyperbolic material calcite, and comparing the different underlying mechanisms of enhancement of near-field radiative heat transfer in calcite and polar dielectric material SiC. Near-field radiative heat transfer between bulk natural hyperbolic materials such as calcites has not been reported before. Here radiation transfer across two flat surfaces of calcite at different temperatures separated by a small gap is studied to analyze the effect of material properties on the underlying mechanisms, and, in turn, the enhanced near-field radiation.

2. Methods, materials, and geometry

We consider two semi-infinite parallel plates, separated by distances comparable to or smaller than the characteristic radiation wavelength. Fig. 1 shows media with in-plane ($\varepsilon_\parallel$) and out-of-plane ($\varepsilon_\perp$) dielectric components. In case of $\varepsilon_\perp = \varepsilon_\parallel$, the schematic represents isotropic materials.

Heat flux as a function of distance between the two flat plates is expressed as [55]:

$$q_{\mathrm{Tot}}(d) = \int_0^\infty \frac{d\omega}{2\pi}[\Theta(\omega, T_2) - \Theta(\omega, T_1)] \times \sum_{i=s,p}\left[\int_0^{\omega/c_o} \frac{d\kappa}{2\pi}\kappa \times \mathcal{T}_i^{\mathrm{prop}}(\omega, d, T_1, T_2) + \int_{\omega/c_o}^{\infty} \frac{d\kappa}{2\pi}\kappa \times \mathcal{T}_i^{\mathrm{evan}}(\omega, d, T_1, T_2)\right] \quad (1)$$

Here, $\Theta(\omega, T)$ stands for probability of states being populated by modes at frequency ω and temperature T, and κ is wavevector parallel to interface. Subscripts s and p stand for TE and TM waves, respectively. This expression is in a general form and applicable to isotropic as well as hyperbolic materials [56]. The Landauer-type formalism composed of $\mathcal{T}_i^{\mathrm{prop}}$ and $\mathcal{T}_i^{\mathrm{evan}}$ represents transmission functions of propagating and evanescent waves, respectively, which is the fraction of total energy carried by the mode κ:

$$\mathcal{T}_i^{\mathrm{prop}}(\omega, d, T_1, T_2) = \frac{\left(1 - |r_{i,1}(T_1)|^2\right)\left(1 - |r_{i,2}(T_2)|^2\right)}{\left|1 - r_{i,1}(T_1) r_{i,2}(T_2) e^{2i\gamma_o d}\right|^2} \quad (2a)$$

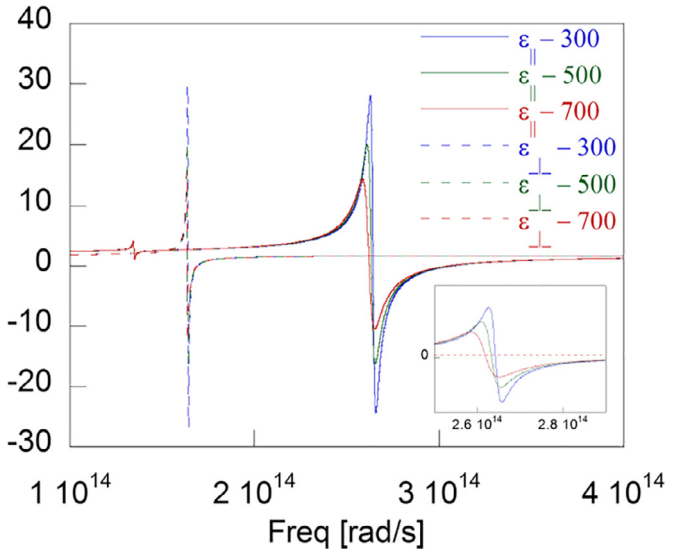

Fig. 2. Real component of in- and out-of-plane dielectric functions of calcite in mid-IR at temperatures of interest. Inset shows variation with respect to temperature of in-plane component around the Type-II frequency band.

$$\mathcal{T}_i^{\mathrm{evan}}(\omega, d, T_1, T_2) = \frac{4\mathrm{Im}(r_{i,1}(T_1))\mathrm{Im}(r_{i,2}(T_2))e^{-2\mathrm{Im}(\gamma_o)d}}{\left|1 - r_{i,1}(T_1) r_{i,2}(T_2) e^{-2\mathrm{Im}(\gamma_o)d}\right|^2} \quad (2b)$$

where r is the Fresnel reflection coefficient at the interface between the materials of interest and vacuum, which can be expressed as [57]:

$$r_{p,j} = \frac{\varepsilon_{\parallel,j}\gamma_o - \gamma_{p,j}}{\varepsilon_{\parallel,j}\gamma_o + \gamma_{p,j}} \quad (3a)$$

$$r_{s,j} = \frac{\gamma_o - \gamma_{s,j}}{\gamma_o + \gamma_{s,j}} \quad (3b)$$

In the expressions above, $\gamma_p (= \sqrt{\varepsilon_\parallel \omega^2/c_o^2 - \varepsilon_\parallel/\varepsilon_\perp \kappa^2})$ and $\gamma_s (= \sqrt{\varepsilon_\parallel \omega^2/c_o^2 - \kappa^2})$ are wavevectors in the direction perpendicular to the interface for p- and s-polarized waves inside the material, and $\gamma_o (= \sqrt{\omega^2/c_o^2 - \kappa^2})$ is the wavevector in vacuum. The numerator of Eq. 2(a) accounts for the portion of transmitted radiative energy by propagating waves through the material interface, and the denominator represents multiple reflections between material interfaces across vacuum gap. In Eq. (2b), $\mathrm{Im}(r_i)$ in the numerator can be interpreted as near-field emission [58] or a quantity proportional to the local density of states (LDOS) [3].

We choose calcite as an example uniaxial hyperbolic material for this study. It has two distinct Reststrahlen bands in mid-IR. Also referred to as lower and upper bands, these Reststrahlen bands exhibit negative dielectric behavior. The lower band spans a frequency range $1.64 \times 10^{14} < \omega < 1.69 \times 10^{14}$ rad/s, and has a Type-I hyperbolic dispersion, i.e., a positive in-plane component and a negative out-of-plane component (see Fig. 2). The upper band, $2.64 \times 10^{14} < \omega < 3.08 \times 10^{14}$ has a Type-II hyperbolic dispersion with a negative in-plane component and a positive out-of-plane component. Also, calcite has a weak in-plane dielectric response due to molecular vibrations around $\omega \sim 1.33 \times 10^{14}$ rad/s. These dielectric components shape the spectral radiation via allowable/forbidden propagating waves inside the hyperbolic material. From the wavevector expressions γ_p $(= \sqrt{\varepsilon_\parallel \omega^2/c_o^2 - \varepsilon_\parallel/\varepsilon_\perp \kappa^2})$ and $\gamma_s (= \sqrt{\varepsilon_\parallel \omega^2/c_o^2 - \kappa^2})$, we can see that in the lower Type I band, propagation of s-polarized (also called ordinary) modes with $\kappa < \sqrt{\varepsilon_\parallel}\omega/c_o$ and all p-polarized (extraordinary) modes are allowed, while in the upper Type-II band propagation is forbid-

Table 1
Fitting-parameters of Lorentz models for calcite and SiC as a function of temperature. Fitting-parameter, Γ, is in unit of *meV* for calcite and cm^{-1} for SiC.

Material	T (K)	A_m (meV)^2	ω_m (meV)	ω_T (1/cm)	ω_L (1/cm)	Γ	ε_∞
SiC	300	–	–	793	969	4.76	6.7
/isotropic	500			787	965	8.5	
	700			781	960.5	12.2	
Calcite/	300	18.4	173.9	–	–	2.02	1.698
asymmetric	500		178.7	–	–	2.93	
	700		172.3	–	–	4.31	
Calcite/in-	300	0.110	88.7	–	–	0.423	1.698
plane	500						
	700						
Calcite/out-	300	1.272	108.0	–	–	0.207	1.647
of-	500		107.9			0.317	
plane	700		107.7			0.420	

den for all s-polarized mode, and is allowable only for waves with $\kappa > \sqrt{\varepsilon_\perp}\omega/c_o$ for p-polarized modes. Note that any mode with $\kappa > \omega/c_o$ inside the material does not propagate in vacuum and is evanescent in near-field because of momentum mismatch with that of light in vacuum (ω/c_o). However, these evanescent modes can tunnel through vacuum to a material nearby, which give rise to enhanced near-field radiative transfer between two materials. Accordingly, in the Type I band, near-field enhancement occurs for $\kappa \in [\omega/c_o, \sqrt{\varepsilon_\parallel}\omega/c_o]$ for s-polarized waves, and for $\kappa \in [\omega/c_o,\infty]$ for p-polarized waves; and in the Type II band, near-field enhancement occurs for $\kappa \in [\sqrt{\varepsilon_\parallel}\omega/c_o, \infty]$ for p-polarized waves only. Since radiation enhancement occurs only in a narrow wavelength band for s-polarized wave, contributions to radiation enhancement are mainly from p-polarized waves.

For comparison, SiC is chosen as a polar dielectric which has been widely studied. Excitation frequency of SPhP at SiC-vacuum interface corresponds to $\sim 1.78 \times 10^{14}$ rad/s within the Reststrahlen band of SiC. SPhPs are transverse surface waves propagating along the interface with large wavevectors that contribute to the enhancement of near-field radiation by increasing the number of coupled resonant modes. Due to transverse optical phonon oscillations in the direction normal to the interface, only p-polarized waves can excite SPhPs. Dielectric properties of calcite and SiC can be modeled with good approximation using the Lorentz oscillator model in infrared frequencies [59,60]. Moreover, calcite and SiC are both durable materials at elevated temperatures: calcite changes its form into CaO with loss of CO_2 at around 1100 K, while SiC withstands even higher temperatures. Since this study covers a relatively large temperature range, temperature dependent optical properties are used, and are expressed for calcite [60] (a two-oscillator model) and SiC [61] as:

$$\varepsilon(\omega) = \varepsilon_\infty + \sum_m \frac{A_m}{\omega_m^2 - \omega^2 - i\Gamma\omega} \tag{4a}$$

$$\varepsilon(\omega) = \varepsilon_\infty\left(1 + \frac{\omega_L^2 - \omega_T^2}{\omega_T^2 - \omega^2 - i\Gamma\omega}\right) \tag{4b}$$

Here, $\omega_T(\omega_L)$ is the transverse (longitudinal) phonon frequency and Γ accounts for losses. ω_m is the frequency of the mth Lorentz oscillator. The fitting-parameters are listed in Table 1. For calcite, the fitting-parameters at room temperature were obtained from ellipsometry data [62], and the fitting-parameters for higher temperatures are derived from dielectric properties reported in ref. [60]. For SiC, considering the fact that variation in ω_T and ω_L of SiC is <2% and the change in Γ is linear with respect to temperature [61], linear interpolation in resonant frequencies is used in calculations within the temperature range of interest (between 300 K and 700 K). Fig. 2 shows dielectric function in both in- and out-of-planes of calcite computed from values in Table 1.

3. Results and discussion

3.1. Transmission coefficients for calcite and comparison with SiC

The transmission function, Eq. (2b), plays a significant role in near-field radiative transfer, and also conveys insightful information. Here we first discuss parameters determining this transmission function. Fig. 3 shows the frequency and wavevector dependency of the transmission function, for calcite (a) and SiC (b), for p-polarized waves. Due to the negligible contribution of s-polarized waves to total heat transfer in hyperbolic bands (~1% in Type-I), only p-polarization is shown. As can be seen, calcite has two regimes with large κd in which the transmission function has non-zero values. These high-κ modes propagate inside calcite within these regimes, and hyperbolic evanescent waves tunnel through vacuum. It is also seen that these regimes are bound by certain κd values, which is related with penetration depth, proportional to $\sim \kappa^{-1}$. Transmission of evanescent modes with small κ values occurs nearly without loss because the penetration depth of these modes is greater than the separation distance, d. Across the same gap, the modes with higher κ values decay faster according to $e^{-2\mathrm{Im}(\gamma_0)d}$ in the transmission expression.

Fig. 3(b) shows for SPhP there are also high-κ modes contributing to the transmission function. Comparison of Fig. 3(a) and (b) indicates there are larger κ values for SPhP that contribute to transmission. This difference can be explained using Fig. 4, which illustrates the imaginary component of Fresnel reflection coefficients for nonradiative p-polarized waves in Eq. 3(a). Fig. 4, as a result of Eq. 3(a) and dielectric properties of hyperbolic material and polar material, indicates that $\mathrm{Im}\, r_p$ in hyperbolic bands cannot exceed 1 for calcite whereas that of SiC has a value over 20 around the resonance frequency. With smaller $\mathrm{Im}\, r_p$ in Eq. 2(b), $\mathcal{T}_p^{\mathrm{evan}}$ approaches 0 at relatively smaller κ value for calcite compared to SiC. The largest wavevectors that enhance energy transfer in calcite is about ~3 times smaller than that in SiC.

Fig. 4 also reveals that for larger κ ($\gg \omega/c$, electrostatic limit), the magnitude of $\mathrm{Im}\, r_p$ within the Reststrahlen bands is a constant of ~0.9 for calcite and ~10 for SiC. Modes with $\kappa \gg \omega/c$ can transfer energy at the near-field, $d < 100$ nm. This implies that at the near-field, enhancement in near-field radiation at shorter distance is not due to the number of modes. Rather, the contribution for the enhancement solely arises from "accessible" larger κ values than that at longer separation as seen in the integral for near-field contribution in Eq. 1 along with constant $\mathrm{Im}\, r_p$ in Eq. 2(b). Thus, near-field enhancement at extreme near-field is dominated by the contribution of the modes with accessible κ values.

3.2. Evaluation of near-field radiative transfer

To analyze the contribution of high-κ modes on radiative transfer in hyperbolic materials, we consider two semi-infinite plates at

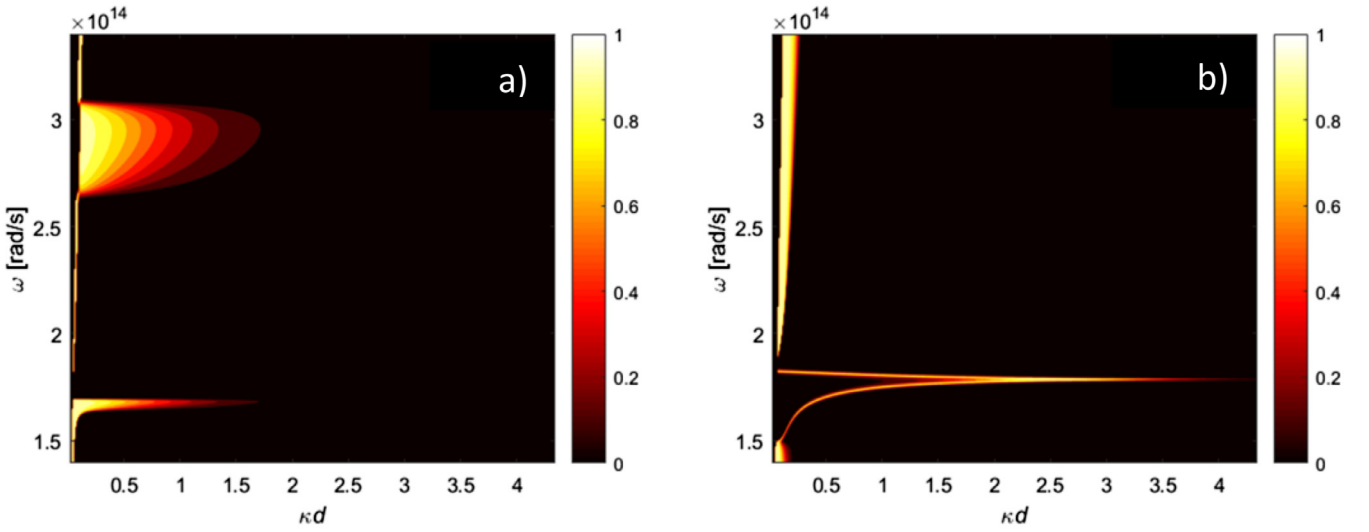

Fig. 3. Transmission function of *p*-polarized waves between materials of calcite (a) and SiC (b) with a separation of 100 nm at 300 K. These plots show the contribution of non-propagating modes in vacuum.

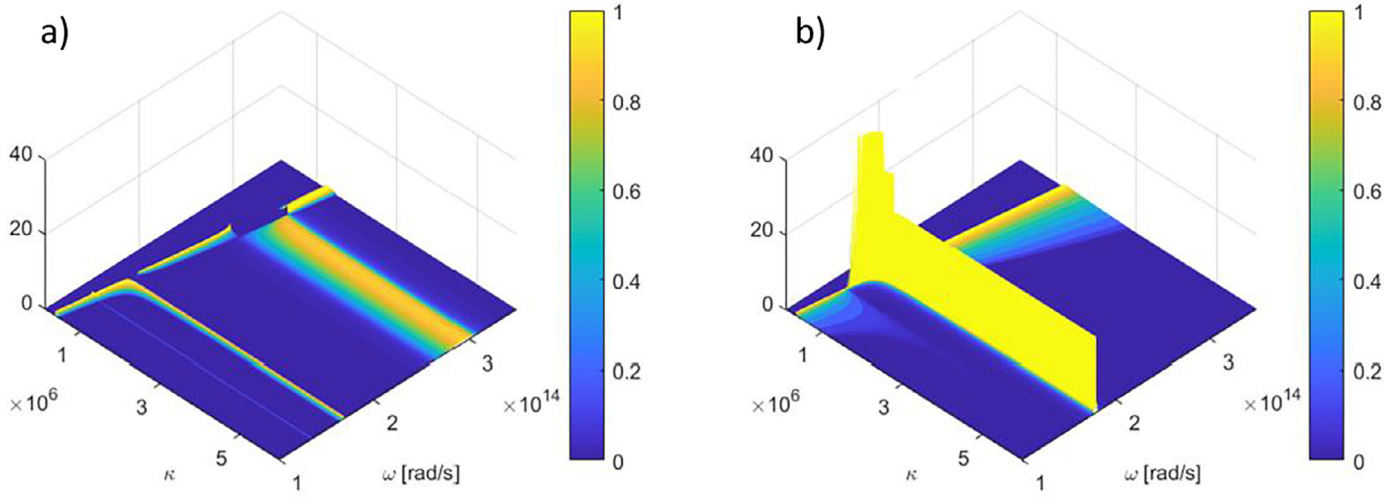

Fig. 4. Imaginary reflection coefficients of nonradiative p-polarized waves for calcite (a) and SiC (b) in Reststrahlen bands. Color bar is from 0 to 1 (for (b), color bar is saturated at 1).

different temperatures separated by a gap. The temperature of one plate is fixed to 300 K, and the temperature difference (ΔT) between two plates is 1 K, 200 K, and 400 K. We validated the code for SiC by comparing our results to the results in [55] and [58]. Fig. 5(a) illustrates the total radiative heat flux (q_{Tot}) as a function of the separation distance between the plates at all temperature differences. At large separation distances (close to 10 μm) when propagating waves in vacuum is the main contribution to radiative heat transfer, calcite transfers slightly more energy. This is a consequence of the term $1-|r_1|^2$ in Eq. 2(a), which represents emissivity of the material. Compared to SiC, calcite has a real component of dielectric function closer to that of air and a lower dielectric loss, which lead to smaller reflectance and in turn, higher emitted radiation.

In the near-field regime, $q_{Tot,calcite}$ increases with the decreasing separation distance due to the tunneling of larger κ-modes supported in the Type-I and -II bands. As discussed above, $e^{-2\kappa d}$ in Eq. 2(b), which governs the transmission function, decays and approaches 0 when $\kappa d \gg 1$. A shorter separation distance allows larger κ to contribute to near-field radiation enhancement. The same reason explains the contribution of SPhP in SiC at shorter distance.

Fig. 5(a) demonstrates radiative heat transfer as a function of separation distance at various temperature differences. In general, $q_{\mathrm{Tot,SiC}} > q_{\mathrm{Tot,calcite}}$ owing to the contribution of the modes with larger κ values (Fig. 3) and larger number of modes than that in calcite at all temperature differences. Fig. 5(b) shows radiation normalized to blackbody radiation at the corresponding temperature difference. At 1 K and 200 K temperature differences, the magnitude of normalized radiative heat transfers for calcite ($q_{Nor,\,calcite}$), is nearly equal (see inset in Fig. 5(b)). This is because on one hand, increasing temperature shifts λ_{max}, the peak wavelength of radiation at the corresponding temperature, towards the Type-II band. Consequently, more populated states, or high-κ modes within the Type-II band enhance near-field radiation. On the other hand, increasing temperature results in broadened Type-II band and weaker dielectric response, as shown in the inset in Fig. 2. This results in smaller $Im\, r_p$, and hence, smaller contribution of hyperbolic evanescent modes to near-field radiation. Increasing ΔT to 400 K decreases the normalized near-field radiation due to even weaker dielectric response as well as λ_{max} moving out of the Type-II band. For SiC, at 1 K difference, the maximum thermal energy excites states around the resonance frequency, 1.78×10^{14} rad/s (10.5 μm), and moves out of this frequency when temperature in-

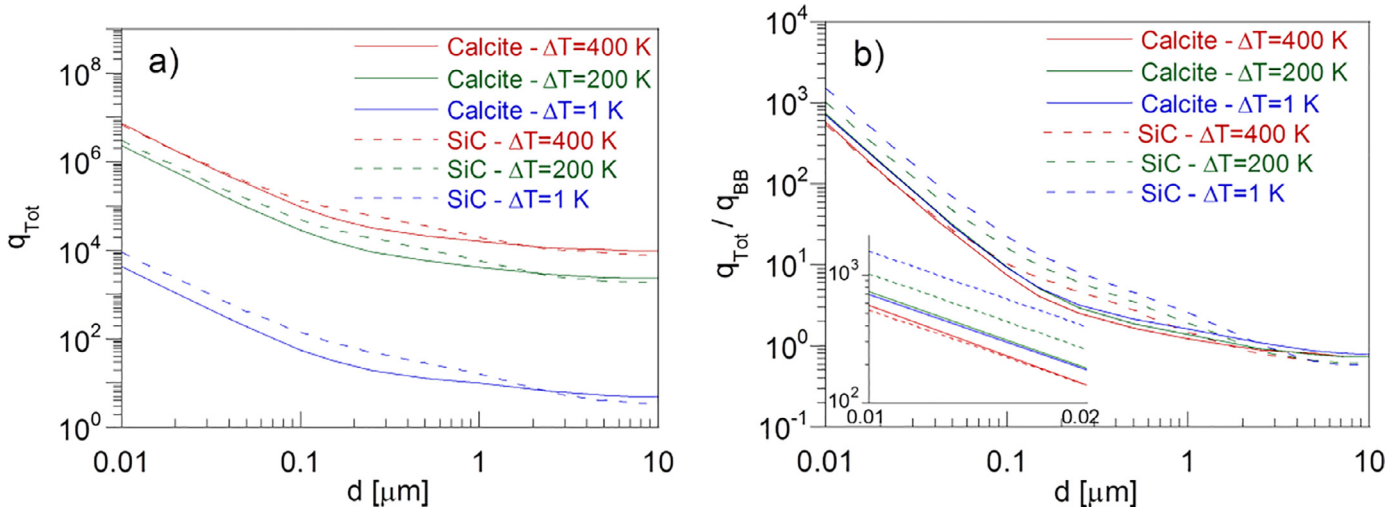

Fig. 5. (a) Total heat flux between two materials, (b) normalized heat transfer to the corresponding blackbody radiation. The inset zooms in extreme near-field range for all cases and is also in log-scale.

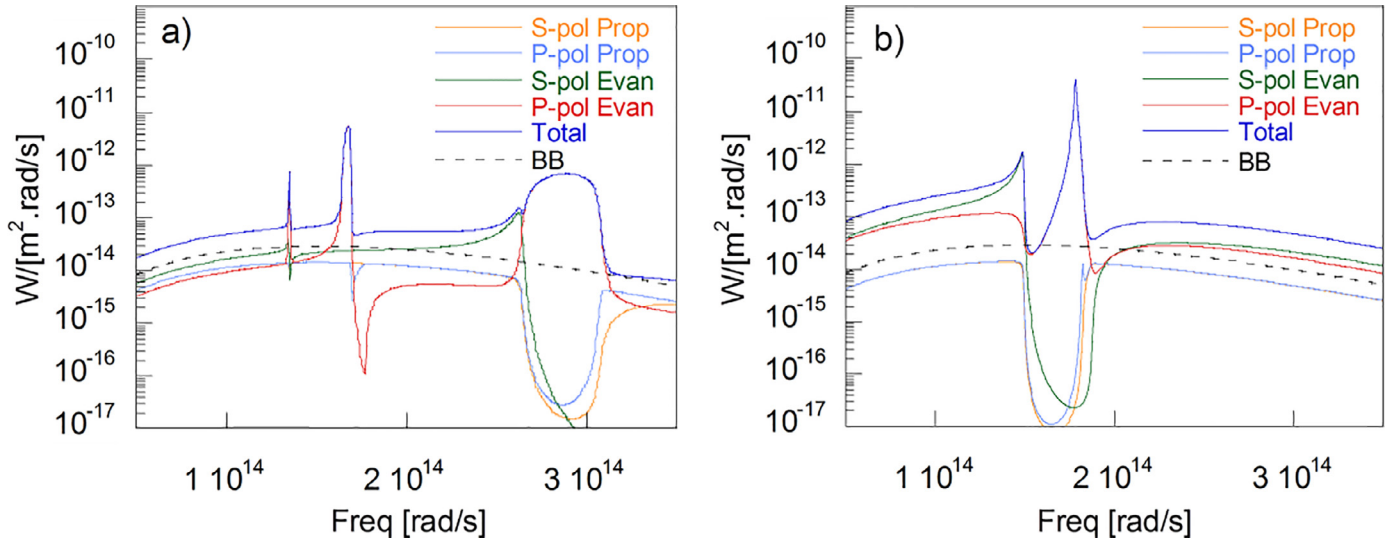

Fig. 6. Spectral heat transfer between calcites (a) and SiC (b) separated by 100 nm for $\Delta T = 1$ K. For completeness, contribution of s- and p-polarized propagating waves are included. BB: blackbody.

creases. Thus, the normalized $q_{Nor,SiC}$ reduces as temperature increases. Similar to calcite, the temperature dependent dielectric properties of SiC also contributes to the decrease of $q_{Nor,\,SiC}$ at larger temperature differences.

Fig. 5(a) and (b) also shows that the increases of both $q_{Tot,SiC}$ and $q_{Tot,calcite}$ from $\Delta T = 200$ K to $\Delta T = 400$ K are not as high as the increases from 1 K to 200 K and $q_{Tot,\,calcite}$ and $q_{Tot,\,SiC}$ are almost the same at the extreme near-field (less than ~20 nm). Inspection of $\mathcal{T}_p^{evan}$ for SiC reveals that at this temperature difference, the frequency of maximum $\mathcal{T}_p^{evan}$ is shifted towards a range where SPhPs have κ values smaller than maximum κ values in dispersion relation of supported polariton modes, which arises from the difference between the resonance frequencies at high temperature. Also, at the resonance frequency for 700 K, wavevectors of polariton modes are nearly half the κ values at the resonance frequency for 300 K due to temperature dependent dielectric properties. Therefore, only the polariton modes with about half the κ values can strongly couple between two surfaces. In contrast, the high-κ modes in calcite within Type-I and -II bands can tunnel through vacuum because each band of the two interfaces for these temperatures still overlaps and supports all the high-κ modes. Thus, calcite has about the same near-field radiation enhancement as SiC at the extreme near-field for $\Delta T = 400$ K.

3.3. Spectral radiative heat transfer

We now further examine the spectral near-field radiative transfer across calcite ($q_{\omega,\,calcite}$) and SiC ($q_{\omega,SiC}$) surfaces. Fig. 6 shows spectral near-field radiative transfer (for all wavevectors) along with near-field contribution of s-polarized evanescent wave ($q_{\omega,s}$) and p-polarized evanescent wave ($q_{\omega,p}$) at a separation distance of 100 nm. A temperature difference $\Delta T = 1$ K is used here. Calcite exhibits three characteristic peaks due to p-polarized waves, and the two of them with higher frequencies are related to the Type-I and Type-II bands. The peak at lower frequencies around $\omega = 1.35 \times 10^{14}$ rad/s is due to a larger value of Im r_p (Fig. 4(a)), which originates from a larger imaginary part of the dielectric constant ($\varepsilon''_{\parallel} \sim 3$). The peak of spectral heat transfer in the Type-I band is higher than that in the Type-II because of λ_{max} falling onto the Type-I band at 300 K. It is also seen that $q_{\omega,p}$ dips near frequencies right to the Type-I band, because $\varepsilon_{\perp} \sim 1$ at those frequencies, leading to small $\gamma_p (= \sqrt{\varepsilon_{\parallel}\omega^2/c_0^2 - \varepsilon_{\parallel}/\varepsilon_{\perp}\kappa^2})$. Another obser-

vation is that $q_{\omega,\,calcite}$ outside hyperbolic bands (and the peak around $\omega = 1.35 \times 10^{14}$) is higher than the spectral blackbody radiation. Each component of the evanescent waves, $q_{\omega,s}$ and $q_{\omega,p}$, mostly remain below blackbody radiation. However, contributions of radiation due to propagating waves (not shown here) are very close to the spectral blackbody radiation. Therefore, $q_{\omega,\,calcite}$, is higher than $q_{\omega,BB}$.

Contributions of s-polarized modes to $q_{\omega,\,\mathrm{calcite}}$ are minimal in the Type-I and Type-II regions, as discussed previously. (The peak to the left of the Type II band is due to bulk resonance. [63]) For frequencies beyond the Type-II band, there is a drastic reduction of the contribution of s-polarization evanescent waves since $0 < \varepsilon_{\parallel} < 1$ (see Fig. 2), meaning that the s-polarized evanescent waves cannot be excited inside the material.

For SiC, only p-polarized waves excite surface polaritons. From Fig. 6(b), it is seen within the Reststrahlen band of SiC, the contribution of s-polarized mode is also minimal. We noticed that $q_{\omega,s}$ and $q_{\omega,p}$ for SiC exceeds the spectral blackbody radiation outside of the Reststrahlen band. This is due to high ε_{SiC} outside of the Reststrahlen band, hence SiC supports large evanescent waves, $\omega/c_o < \kappa < \sqrt{\varepsilon}\omega/c_o$, contributing to near-field radiation for both polarizations. Fig. 6(b) also shows that $q_{\omega,\mathrm{SiC}}$ at resonance frequency is higher than that due to the hyperbolic modes in calcite, because, as discussed above, modes with relatively larger κ values in SiC can contribute near-field radiation.

4. Conclusion

In this study, we carried out analyses on radiative heat transfer of natural hyperbolic material, calcite, and compared to that of a polar material SiC. Our study reveals that, the high-κ modes within the hyperbolic bands are responsible for the largely enhanced near-field radiation. Comparison of calcite with SiC illustrates the significance of the high-κ modes in calcite vs. surface polariton modes in SiC in their contributions to near-field radiation enhancement, for temperature differences ranging from 1 K to 400 K. We also noticed that the contribution of high-κ modes in calcite to near-field radiation is comparable to that of surface polaritons in SiC. However, in general, the contribution of high-κ modes over the entire spectrum is not as high as the polariton modes in SiC due to contributions of wavevectors with a smaller range. On the other hand, at very near-field, the enhancement from calcite is about the same as that from SiC at a large temperature difference of 400 K. This is because the resonance frequencies of SPhPs in SiC for these temperatures shift and polariton couplings take place only at smaller κ values. In contrast, despite of the shift with temperature in Type-I and -II bands in calcite, each band at these temperatures still mainly overlaps. The results of these analyses will be helpful in the search of hyperbolic materials that can enhance near-field radiative transfer.

Funding

Support to this work by the National Science Foundation (1804377-CBET) is gratefully acknowledged.

References

[1] Polder D, Hove MV. Theory of radiative heat transfer between closely spaced bodies. Phys Rev B 1971;4:3303.
[2] Loomis JJ, Maris HJ. Theory of heat transfer by evanescent electromagnetic waves. Phys Rev B 1994;50:18517.
[3] Pendry JB. Radiative exchange of heat between nanostructures. J Phys: Condens Matter 1999;11:6621.
[4] Joulain K, Mulet JP, Marquier F, Carminati R, Greffet JJ. Surface electromagnetic waves thermally excited: radiative heat transfer, coherence properties and Casimir forces revisited in the near field. Surf Sci Rep 2005;57:59–112.
[5] Rousseau E, Siria A, Jourdan G, Volz S, Comin F, Chevrier J, Greffet JJ. Radiative heat transfer at the nanoscale. Nat Photonics 2009;3:514–17.
[6] Shen S, Narayanaswamy A, Chen G. Surface phonon polaritons mediated energy transfer between nanoscale gaps. Nano Lett 2009;9:2909–13.
[7] Ottens RS, Quetschke V, Wise S, Alemi AA, Lundock R, Mueller G, Reitze DH, Tanner DB, Whiting BF. Near-field radiative heat transfer between macroscopic planar surfaces. Phys Rev Lett 2011;107:014301.
[8] Watjen J I, Zhao B, Zhang Z M. Near-field radiative heat transfer between doped-Si parallel plates separated by a spacing down to 200 nm. Appl Phys Lett 2016;109:203112.
[9] Bernardi MP, Milovich D, Francoeur M. Radiative heat transfer exceeding the blackbody limit between macroscale planar surfaces separated by a nanosize vacuum gap. Nat Commun 2016;7:12900.
[10] St-Gelais R, Zhu L, Fan S, Lipson M. Near-field radiative heat transfer between parallel structures in the deep subwavelength regime. Nat Nanotechnol 2016;11:515–19.
[11] Song B, Thompson D, Fiorino A, Ganjeh Y, Reddy P, Meyhofer E. Radiative heat conductances between dielectric and metallic parallel plates with nanoscale gaps. Nat Nanotechnol 2016;11:509–14.
[12] Lang S, Sharma G, Molesky S, Kranzien PU, Jalas T, Jacob Z, Petrov AY, Eich M. Dynamic measurement of near-field radiative heat transfer. Sci Rep 2017;7:13916.
[13] Ito K, Nishikawa K, Miura A, Toshiyoshi H, Iizuka H. Dynamic modulation of radiative heat transfer beyond the blackbody limit. Nano Lett 2017;17:4347–53.
[14] Ghashami M, Geng H, Kim T, Iacopino N, Cho SK, Park K. Precision measurement of phonon-polaritonic near-field energy transfer between macroscale planar structures under large thermal gradients. Phys Rev Lett 2017;120:175901.
[15] Fiorino A, Thompson D, Zhu L, Song B, Reddy P, Meyhofer E. Giant enhancement in radiative heat transfer in sub-30 nm gaps of plane parallel surfaces. Nano Lett 2018;18(6):3711–15.
[16] Chen K, Santhanam P, Fan S. Near-field enhanced negative luminescent refrigeration. Phys Rev Appl 2016;6:024014.
[17] Hsu WC, Tong JK, Liao B, Huang Y, Boriskina SV, Chen G. Entropic and near–field improvements of thermoradiative cells. Sci Rep 2016;6:34837.
[18] Strandberg R. Theoretical efficiency limits for thermoradiative energy conversion. J Appl Phys 2015;117:055105.
[19] Guha B, Otey C, Poitras CB, Fan S, Lipson M. Near-field radiative cooling of nanostructures. Nano Lett 2012:12.
[20] Jones AC, Raschke MB. Thermal infrared near-field spectroscopy. Nano Lett 2012;12(3):1475–81.
[21] Babuty A, Joulain K, Chapuis PO, Greffet JJ, Wilde YD. Blackbody spectrum revisited in the near field. Phys Rev Lett 2013;110:146103.
[22] O'Callahan BT, Lewis WE, Jones AC, Raschke MR. Spectral frustration and spatial coherence in thermal near-field spectroscopy. Phys Rev B 2014;89:245446.
[23] Laroche M, Carminati R, Greffet JJ. Near-field thermophotovoltaic energy conversion. J Appl Phys 2006;100:063704.
[24] Khandekar C, Messina R, Rodriguez AW. Near-field refrigeration and tunable heat exchange through four-wave mixing. AIP Adv 2018;8:055029.
[25] Otey C R, Fan S. Thermal rectification through Vacuum. Phys Rev Lett 2010;104:154301.
[26] Basu S, Francoeur M. Near-field radiative transfer based thermal rectification using doped silicon. Appl Phys Lett 2011;98:113106.
[27] Wang LP, Zhang ZM. Thermal rectification enabled by near-field radiative heat transfer between intrinsic silicon and a dissimilar material. Nanosclae Microscale Thermophys Eng 2013;17:4.
[28] Elzouka M, Ndao S. High temperature near-field nanothermomechanical rectification. Sci Rep 2017;7:44901.
[29] Ben-Abdallah P, Biehs SA. Thermotronics: towards nanocircuits to manage radiative heat flux. Z Naturforsch 2017;72:151–62.
[30] Ben-Abdallah P, Biehs SA. Towards Boolean operations with thermal photons. Phys Rev B 2016;94:241401.
[31] Shi J, Liu B, Li P, Ng L-Y, Shen S. Near-field energy extraction with hyperbolic metamaterials. Nano Lett 2015;15:1217–21.
[32] Messina R, Ben-Abdallah P, Guizal B, Antezza M, Biehs S-A. Hyperbolic waveguide for long-distance transport of near-field heat flux. Phys Rev B 2016;94:104301.
[33] Biehs S-A, Tschikin M, Messina R, Ben-Abdallah P. Super-Planckian near-field thermal emission with phonon-polaritonic hyperbolic metamaterials. Appl Phys Lett 2013;102:131106.
[34] Biehs S-A, Ben-Abdallah. Near-field heat transfer between multilayer hyperbolic metamaterials. Z Naturforsch 2017;72a:115–27.
[35] Liu X L, Zhang R Z, Zhang Z M. Near-field thermal radiation between hyperbolic metamaterials: graphite and carbon nanotubes. Appl Phys Lett 2013;103:213102.
[36] Liu X, Xuan Y. Super-Planckian thermal radiation enabled by hyperbolic surface phonon polaritons. Sci China Tech Sci 2016;59:1680–6.
[37] Shekhar P, Atkinson J, Jacob Z. Hyperbolic metamaterials: fundamentals and applications. Nano Convergence 2014;1:14.
[38] Lu D, Kan JJ, Fullerton EE, Liu Z. Enhancing spontaneous emission rates of molecules using nanopatterned multilayer hyperbolic metamaterials. Nat Nanotechnol 2014;9:48–53.
[39] Korobkin D, Neuner B III, Fietz C, Jegenyes N, Ferro G, Shvets G. Measurements of the negative refractive index of sub-diffraction waves propagating in an indefinite permittivity medium. Opt Express 2010;18:22734–46.
[40] Galfsky T, Krishnamoorthy HNS, Newman W, Narimanov E E, Jacob Z, Menon V M. Active hyperbolic metamaterials: enhanced spontaneous emission and light extraction. Optica 2015;2:62–5.

[41] Liu Z, Lee H, Xiong Y, Sun C, Zhang X. Far-field optical hyperlens magnifying sub-diffraction-limited objects. Science 2007;315:1686.
[42] Cortes CL, Newman W, Molesky S, Jacob Z. Quantum nanophotonics using hyperbolic metamaterials. J Opt 2012;16:129501.
[43] Narimanov EE, Kildishev AV. Naturally hyperbolic. Nat Photonics 2015;9:214–16.
[44] Dai S, Ma Q, Andersen T, Mcleod AS, Fei Z, Liu MK, Wagner M, Watanabe K, Taniguchi T, Thiemens M, Keilmann F, Herrero PJ, Fogler MM, Basov DN. Subdiffractional focusing and guiding of polaritonic rays in a natural hyperbolic material. Nat Commun 2015;6:6963.
[45] Li O, Lewin M, Kretinin A, Caldwell JD, Novoselov KS, Taniguchi T, Watanabe K, Gaussmann F, Taubner T. Hyperbolic phonon-polaritons in boron nitride for near-field optical imaging and focusing. Nat Commun 2015;6:7507.
[46] Gall J L, Olivier M, Greffet J J. Experimental and theoretical study of reflection and coherent thermal emission by a SiC grating supporting a surface-phonon polariton. Phys Rev B 1997;55:10105.
[47] Hillebrand R, Taubner T, Keilmann F. Phonon-enhanced light-matter interaction at the nanometre scale. Nature 2002;418:159–62.
[48] Mirlin DN. Surface phonon polaritons in dielectrics and semiconductors. Mod Probl Condens Matter Sci 1982;1:3–67.
[49] Caldwell JD, Lindsay L, Giannini V, Vurgaftman I, Reinecke TL, Maier S A, Glembocki O J. Low-loss, infrared and terahertz nanophotonics using surface phonon polaritons. Nanophotonics 2015;4:44–68.
[50] Francoeur M, Mengüç MP, Vaillon R. Spectral tuning of near-field radiative heat flux between two thin silicon carbide films. J Phys D 2010;43:075501.
[51] Edalatpour S, Francoeur M. Size effect on the emissivity of thin films. J Quant Spectrosc Rad Transf 2013;118:75–85.
[52] Ito K, Matsui T, Iizuka H. Thermal emission control by evanescent wave coupling between guided mode of resonant grating and surface phonon polariton on silicon carbide plate. Appl Phys Lett 2014;104:051127.
[53] Didari A, Mengüç MP. Analysis of near-field radiation transfer within nano–gaps using FDTD method. J Quant Spectrosc Rad Transf 2014;146:214–26.
[54] Greffet JJ, Carminati R, Joulain K, Mulet JP, Mainguy S, Chen Y. Coherent emission of light by thermal sources. Nature 2002;416:61–4.
[55] Biehs SA, Greffet JJ. Mesoscopic description of radiative heat transfer at the nanoscale. Phys Rev Lett 2010;105:234301.
[56] Biehs SA, Ben-Abdallah P, Rosa FSS, Joulain K, Greffet JJ. Nanoscale heat flux between nanoporous materials. Optics Exp 2011;19:A1088–103.
[57] Yeh P. Optical waves in layered media. 2nd ed. Wiley-Interscience; 2005.
[58] Mulet JP, Joulain K, Carminati R, Greffet JJ. Enhanced radiative heat transfer at nanometric distances. Microscale Thermophys Eng 2002;6:209–22.
[59] Herve A, Drevillon J, Ezzahri Y, Joulain K, Meneses DDS, Hugonin JP. Temperature dependence of a microstructured SiC coherent thermal source. J Quant Spectrosc Rad Transf 2016;180:29–38.
[60] Sakuri T, Sato T. Temperature dependence of vibrational spectra in calcite by means of emissivity measurement. Phys Rev B 1971;4:583.
[61] Marquier F, Joulain K, Mulet JP, Carminati R, Greffet JJ. Coherent spontaneous emission of light by thermal sources. Phys Rev B 2004;69:155412.
[62] Thompson DW, DeVries MJ, Tiwald TE, Woolam JA. Determination of optical anisotropy in calcite from ultraviolet to mid-infrared by generalized ellipsometry. Thin Solid Films 1998;313:341–6.
[63] Rousseau E, Laroche M, Greffet JJ. Asymptotic expressions describing radiative heat transfer between polar materials from the far-field regime to the nanoscale regime. J Appl Phys 2012:111–014311.